Research on Engineering Structures & Materials
www.jresm.org
Research Group

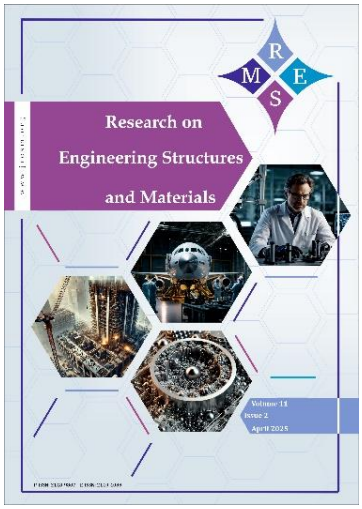

Fabrication of a polymeric film supported by nanoparticles prepared by pulsed laser ablation method

Rana S. Mahmood, Suhad Aloon Abdullh

Online Publication Date: 20 July 2026

URL: http://www.jresm.org/archive/resm2026-1530ma0223rs.html
DOI: http://dx.doi.org/10.17515/resm2026-1530ma0223rs

Journal Abbreviation: *Res. Eng. Struct. Mater.*

To cite this article
Mahmood R S, Abdullh S A. Fabrication of a polymeric film supported by nanoparticles prepared by pulsed laser ablation method. *Res. Eng. Struct. Mater.*, 2026; 12(5): 3651-3663.

Disclaimer
All the opinions and statements expressed in the papers are on the responsibility of author(s) and are not to be regarded as those of the journal of Research on Engineering Structures and Materials (RESM) organization or related parties. The publishers make no warranty, explicit or implied, or make any representation with respect to the contents of any article will be complete or accurate or up to date. The accuracy of any instructions, equations, or other information should be independently verified. The publisher and related parties shall not be liable for any loss, actions, claims, proceedings, demand or costs or damages whatsoever or howsoever caused arising directly or indirectly in connection with use of the information given in the journal or related means.

Published articles are freely available to users under the terms of Creative Commons Attribution - NonCommercial 4.0 International Public License, as currently displayed at here (the "CC BY - NC").

Research on Engineering Structures & Materials
www.jresm.org
Research Group

Research Article

Fabrication of a polymeric film supported by nanoparticles prepared by pulsed laser ablation method

Rana S. Mahmood [*,a], Suhad Aloon Abdullh [b]

Ministry of Education, Diyala Education Directorate, Diyala Iraq

Article Info

Article History:

Received 23 Feb 2026

Accepted 16 July 2026

Keywords:

Polymer;
Polyethylene glycol;
AgNPs;
AuNPs;
Nanoparticles;
Laser ablation

Abstract

Biocompatible polymer membranes are currently in increasing demand, especially those containing homogeneously distributed nanoparticles for medical applications. This research aims to develop a clean and effective approach using pulsed laser ablation. Silver nanoparticles (AgNPs) and gold nanoparticles (AuNPs) have been used as antibacterial agents in the consumer goods, cosmetics, and food industries. In this work, silver and gold nanoparticles were synthesized in a polyethylene glycol (PEG) medium using pulsed laser ablation. The fabricated films were characterized using Fourier transform infrared spectroscopy (FTIR) to identify functional groups, UV–Vis spectroscopy to analyze optical properties, and field emission scanning electron microscopy (FESEM) to examine surface morphology and nanoparticle distribution. In addition, the antibacterial activity was evaluated using the agar diffusion method. The results showed spherical nanoparticles with a polydisperse size distribution, indicating that the medium supports the production of small, well-dispersed nanoparticles, which was reflected in the uniform surface morphology and enhanced antibacterial performance. The results showed spherical nanoparticles with a polydisperse size distribution, indicating that the medium supports the production of small and stable silver nanoparticles, which contributed to reduced aggregation and exhibited enhanced antibacterial performance. The produced silver and gold nanoparticles have been successfully used as an antibacterial agent, as experimentally demonstrated using (Staphylococcus aureus), Enterococcus faecalis, Escherichia coli, and Klebsiella pneumoniae). The results showed that the manufactured silver and gold nanoparticles exhibited significant antibacterial activity against Staphylococcus aureus, with larger zones of inhibition observed compared to other tested samples, indicating an enhanced antibacterial activity based on the results of the assay.

© 2026 MIM Research Group. All rights reserved.

1. Introduction

Polymeric nanocomposite films reinforced with nanoparticles have attracted significant attention due to their enhanced optical, mechanical, and thermal properties, which make them suitable for applications in sensing, biomedical devices, and optoelectronic technologies. Among the various nanoparticle synthesis techniques, pulsed laser ablation (PLA) offers a clean and efficient method for producing high-purity nanoparticles without chemical contaminants. Therefore, this study focuses on the fabrication of a polymeric film supported by nanoparticles prepared via the pulsed laser ablation method and the investigation of its structural and functional properties [1]. Their unique optical, biological, and electrical properties make them promising materials for improving the performance of advanced functional devices and polymer-based nanocomposites [2].
Polyethylene glycol (PEG) is a hydrophilic and biocompatible semi-crystalline polymer synthesized through the polymerization of ethylene glycol monomers. In the present study, PEG was selected

*Corresponding author: ranasaadmahmood82@gmail.com
[a]orcid.org/0009- 0002 - 7866 - 3026; [b]orcid.org/ 0009- 0002 - 0165 - 0219
DOI: http://dx.doi.org/10.17515/resm2026-1530ma0223rs

as the polymer matrix because of its low toxicity, excellent water solubility, film-forming capability, and strong compatibility with nanoparticles, which support homogeneous nanoparticle dispersion and improve the stability and functional performance of the fabricated nanocomposite film. The unique properties of polyethylene glycol (PEG), including its low toxicity, biocompatibility, and hydrophilic nature, make it a suitable polymer matrix for nanoparticle-based nanocomposite films. These characteristics promote stable nanoparticle dispersion and improve the interaction between the polymer and nanoscale fillers. In polymer nanocomposites, fillers with dimensions below 100 nm are incorporated to enhance the structural, optical, and functional properties of the resulting material [3,4]. Metal nanoparticles such as silver nanoparticles (AgNPs) and gold nanoparticles (AuNPs) have attracted considerable attention because their optical, electrical, and catalytic properties differ significantly from those of bulk materials [5]. In the present study, these nanoparticles were incorporated into the PEG matrix to enhance the functional properties of the fabricated nanocomposite film. In particular, AgNPs are well known for their strong antimicrobial activity against harmful microorganisms, while AuNPs contribute to improved optical stability and surface-related properties, making both AgNPs and resulting film potentially interesting for future advanced biomedical and functional applications, as suggested literature context [6]. Gold nanoparticles (AuNPs) possess unique optical, physicochemical, and biological properties, in addition to a large surface area and low toxicity, making them highly attractive for biomedical and biotechnological applications [7,8]. In the present study, AuNPs were incorporated into the PEG-based film to improve the stability, surface activity, and functional performance of the antibacterial nanocomposite system. Their high surface reactivity and biocompatibility also support effective interaction with the polymer matrix, which is important for enhancing the overall properties of PEG-based antibacterial films [9–12]. Gold nanoparticles (AuNPs) are widely applied in nanocomposite systems due to their strong surface plasmon resonance, high surface reactivity, and excellent biocompatibility, which make them particularly effective in modifying polymer matrices such as PEG for biomedical and antibacterial applications. In PEG-based antibacterial films, AuNPs contribute to improving surface interactions and functional stability of the composite, thereby enhancing its overall performance in biomedical environments. In this context, the integration of AuNPs into the polymer matrix is specifically motivated by their ability to enhance the structured stability and antibacterial efficacy of the resulting nanocomposite, providing a tailored material design that is frequently discussed in literature for potential biomedical applications [13]. Furthermore, this study focuses on the effectiveness of the pulsed laser ablation method in preparing these nanocomposites, specifically examining how the incorporation of AgNPs and AuNPs into the PEG matrix influences the optical and antibacterial properties of the fabricated films [11-13]. Silver nanoparticles (AgNPs) are of particular relevance in polymer-based antibacterial nanocomposites due to their strong and well-documented antimicrobial activity arising from silver ion release and their ability to disrupt bacterial cell membranes. In PEG-based composite films, AgNPs are therefore primarily employed to impart antibacterial functionality and improve the protective performance of the material for potential biomedical-related applications as highlighted in the literature [14–16]

2. Experimental Section

2.1 Materials

Polyethylene glycol (PEG), with the molecular formula $HO(C_2H_4O)_nH$ and a molecular weight in the range of 3500–4000 $g{\cdot}mol^{-1}$, was used in this study as the polymer matrix. The PEG was utilized in solid form (pellets from LOBA CHEMIE PVT.LTD/ India). In addition, silver and gold alloys were analyzed using an energy-dispersive X-ray fluorescence (ED-XRF) spectrometer (XEPOS model/ made in Germany) to determine their elemental composition and purity. The measured purities of the silver and gold alloys were found to be 98.99% and 99%, respectively.

2.2 Synthesis of PEG/ Ag and Au Nanoparticles

Initially, high-purity gold and silver plates (99.9%) were used as ablation targets and were ultrasonically cleaned in ethanol, acetone, and deionized water (DIW) for 10 min each to remove surface contaminants. Each target was then placed at the bottom of a separate glass container

containing 3 mL of DIW. The targets were irradiated using a pulsed Nd:YAG laser operating at a fundamental wavelength of 1064 nm, pulse duration of 10 ns, repetition rate of 1 Hz, and pulse energy of 500 mJ, corresponding to a fluence of 0.5 J/cm^2. The laser beam (6 mm in diameter) was focused onto the target surface using a convex lens with a focal length of 10 cm. A total of 1000 pulses were applied, and the ablation process was carried out for 30 min to generate colloidal gold and silver nanoparticles dispersed in DIW. For the preparation of nanocomposite films, polyethylene glycol (PEG) solution was used as the polymer matrix. Briefly, 2 g of PEG was dissolved in 35 mL of distilled water under magnetic stirring at 70 °C for 3 h until a homogeneous, bubble-free solution was obtained. The prepared colloidal solutions containing AuNPs and AgNPs were then separately added to the PEG solution under continuous stirring to ensure uniform dispersion of nanoparticles within the polymer matrix. The resulting nanocomposite mixtures were poured into clean, leveled glass Petri dishes and allowed to dry under controlled ambient laboratory conditions (25 ± 2 °C, relative humidity ~40–50%) until complete solvent evaporation. This solution casting process resulted in uniform PEG/AuNP and PEG/AgNP composite films with an average thickness of 125 μm. The nanoparticle was incorporated by adding 3mL of the colloidal solution to the PEG matrix (2 g in 35mL) The FESEM analysis confirmed the uniform distribution of nanoparticles throughout the polymer matrix, which ensures consistent optical and antibacterial performance. Finally, the obtained films were carefully peeled from the dishes and stored in a desiccator at room temperature to prevent moisture absorption and preserve their structural stability.

2.3 Antimicrobial Activity Tests

Blood agar was used to cultivate isolates of Klebsiella pneumoniae, Escherichia coli, Enterococcus faecalis, and Staphylococcus aureus. The bacterial suspension density was standardized using a 0.5 McFarland turbidity standard to achieve a cell concentration of approximately 1.5× 108 CFU/mL, Regarding the medium preparation, 38 grams were dissolved in one liter of distilled water to create this medium, which was then autoclaved at 121 degrees Celsius and 15 pounds of pressure for 15 minutes. It was then cooled, transferred into sterile plates, and stored in the refrigerator until it was needed.

To prepare the bacterial suspension, distinct bacterial colonies were transferred via a sterile inoculation loop into tubes containing brain-heart infusion broth. The tubes were incubated at 37 °C for 18 to 24 hours. Next, a sterile swab was utilized to uniformly inoculate the bacterial suspension onto Mueller-Hinton agar plates, which were then left to dry under aseptic conditions. Wells were prepared in the culture media using a sterile cork borer. Utilizing a micropipette, a 100 μL aliquot of each tested concentration (100, 75, 50, 25, and 12.5 μg/mL) was introduced into each well. Finally, the diameters of the zones of inhibition were measured to evaluate the antimicrobial efficacy of each concentration.

2.4 Characterization Techniques

Absorption spectra and Surface Plasmon Resonance (SPR) were recorded for colloids with UV-ViS spectrophotometer (Double Beam 1800 UV, Shimadzu, Japan) manufactured in (Shimadzu, Japan) for the purpose of knowing the effective aggregates, FTIR test: using type the IR Affinity-1CE (FTIR) spectrophotometer, Shimadzu, Japan.

3. Results and Discussions

3.1. Surface Chemistry (FT-IR)

The produced Ag NPs and Au NPs may interact with the PEG molecules. In Figure 3, the FTIR spectra of both pure PEG and PEG-AuNPs are displayed. A wide absorption band at 3437 cm^{-1} was observed, which corresponds to the O–H stretching vibration of hydroxyl groups inside the polymer structure, because PEG is generated from ethylene glycol. Furthermore, at 2873.94 cm^{-1}, the bending vibrations linked to O–C–H, C–C–H, and C–O–H groups were detected, and at 1348.24 cm^{-1}, the stretching vibrations of methylene groups were noted.

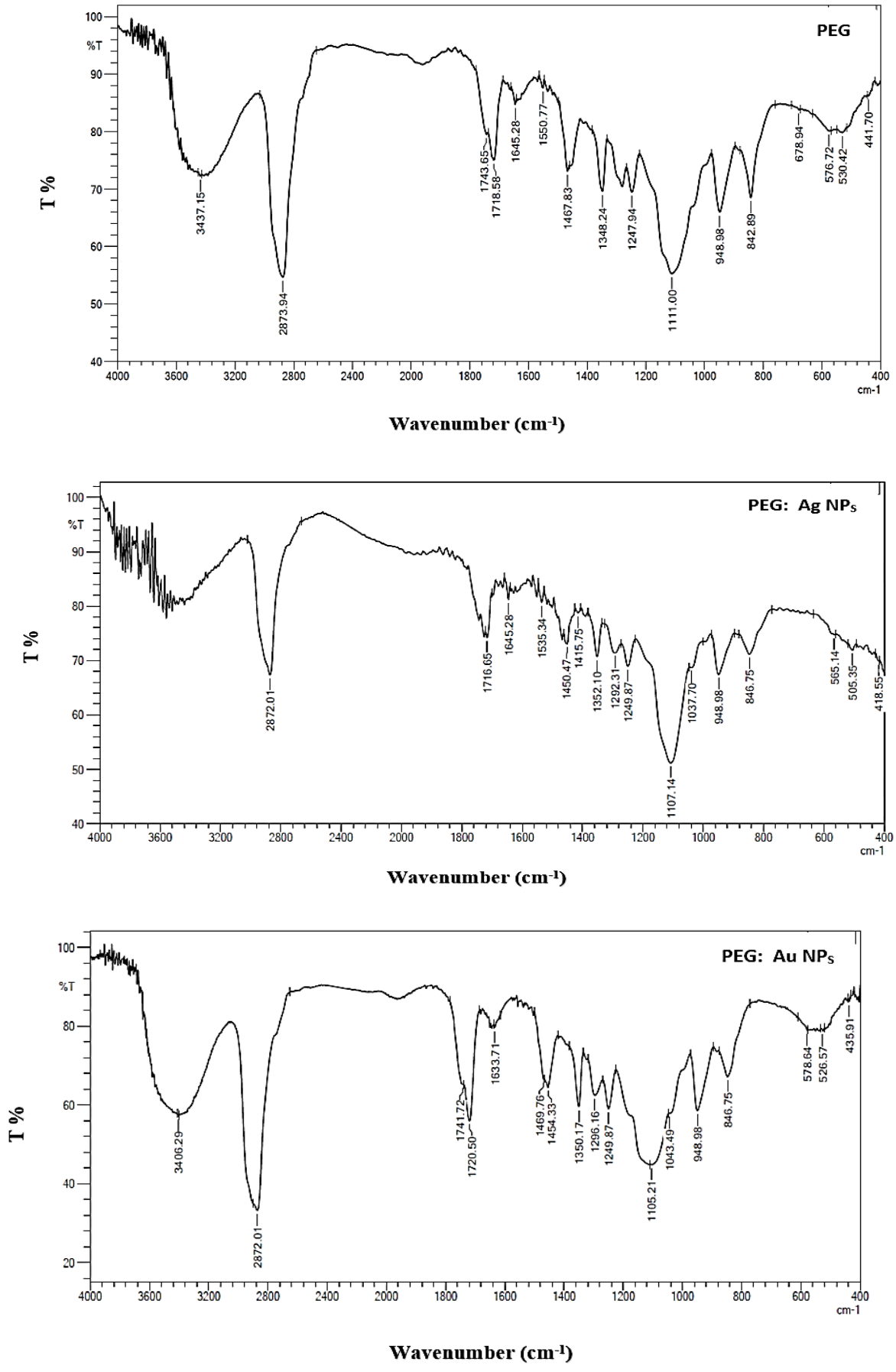

Fig. 1. FTIR spectra of (a) pure PEG, (b) PEG: Ag NP_s and (c) PEG: Au NP_s composites

Near 1111 cm^{-1}, the distinctive ether C–O–C stretching band was seen, along with –CH– out-of-plane bending vibrations at around 948.98 cm^{-1}. Characteristic spectral properties of PEG are supported by these bands. Possible changes in the chemical environment of PEG functional groups following nanoparticle production are indicated by a vibrational band at 1645.28 cm^{-1} in the PEG-AuNP spectra. In addition, the interactions between the metal nanoparticles and the oxygen-containing functional groups of the PEG chains could explain the peaks at 526.57 and 418.55 cm^{-1}. The results of this study provide credence to the idea that polyethylene glycol (PEG) could play a stabilizing and lowering role in the creation of nanoparticles through interactions with their surfaces. However, no clear proof of specific van der Waals interactions or chemical bonding mechanisms can be drawn from the FTIR results alone; further characterization techniques are needed FT-IR Surface Chemistry [17,18].

3.2 Optical Analyses

The UV–Vis spectra confirmed the formation of Ag NPs within the PEG polymeric matrix through the appearance of a distinct SPR band at 430 nm, which is characteristic of silver nanoparticles. Surface plasmon resonance arises from the collective oscillation of conduction electrons on the nanoparticle surface when interacting with incident light. The position and intensity of the SPR band depend on nanoparticle size, shape, distribution, and the surrounding dielectric environment. The PEG membrane itself exhibited low absorbance in the 100–1100 nm region [19], while increased absorption below 300 nm, with a maximum at 298 nm, is attributed to the intrinsic absorption of the polymer and trapped water molecules within the matrix. The emergence of the SPR peak at 430 nm therefore demonstrates the successful reduction of Ag^{+} ions and stabilization of Ag nanoparticles in the PEG medium [20]. The UV-Vis spectrum of the gold nanoparticles also showed an absorption peak at 529 nm (Fig. 2.). This absorption peak at 529 nm is attributed to the SPR property of the gold nanoparticles [21]. Other researchers have observed a similar peak [23,24]. The chemical environment and preparation method play a crucial role in determining the size and shape of the nanoparticles [19].

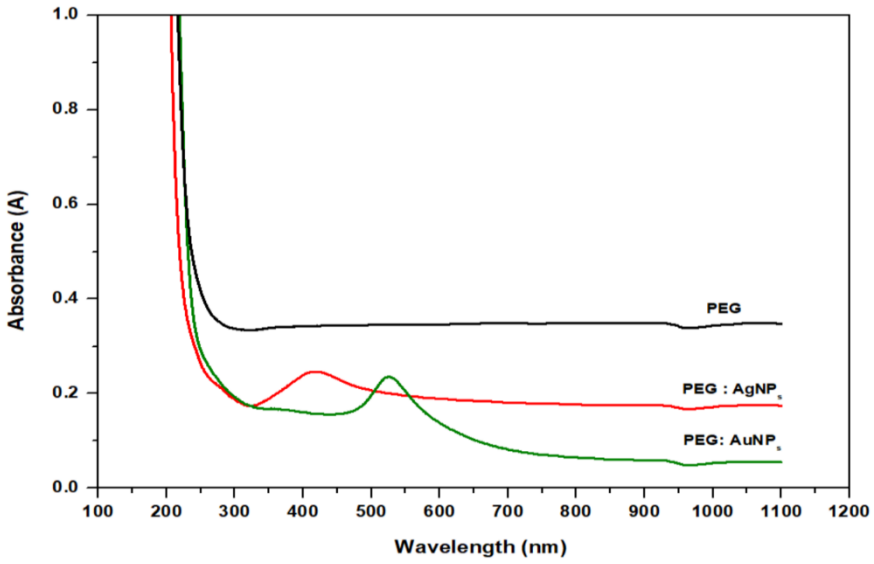

Fig. 2. UV-vis absorption specta of PEG, PEG:$AgNP_s$ and PEG:$AuNP_s$

The optical band gap energies of pure PEG and PEG films doped with Ag and Au nanoparticles were determined using the Tauc relation by extrapolating the linear portion of the $(\alpha h\nu)^{1/2}$ versus photon energy ($h\nu$) plots (Fig. 3). The intercept of this linear region with the energy axis (at $\alpha = 0$) corresponds to the optical band gap, indicating an indirect allowed electronic transition in the investigated films. This model was selected because the $(\alpha h\nu)^{1/2}$ versus ($h\nu$) plots exhibited better linearity compared to the $((\alpha h\nu)^{1/2})$ plot, which is characteristic of direct transition. This confirms that the indirect transition model provides a more accurate representation of the optical band gap for these specific nanocomposites. In indirect band gap materials, electronic transitions involve a change in momentum and therefore require phonon participation, which reduces the probability

of radiative recombination and suppresses direct photon emission. The obtained results show that the optical band gap of pure PEG (4.76 eV) decreases upon incorporation of nanoparticles, reaching 4.0 eV for Ag-doped films and 3.5 eV for Au-doped films. This reduction confirms that nanoparticle incorporation significantly modifies the electronic structure of the PEG matrix.

This behavior can be attributed to the formation of localized electronic states within the band structure, introduced by the presence of metallic nanoparticles. These states act as defect-like energy levels within the band gap, facilitating electronic transitions at lower energies and thereby reducing the effective optical band gap. Such modifications are consistent with previous reports indicating that inorganic nanoparticle fillers can strongly influence the optical and electronic properties of polymer matrices [24–26]. The observed decrease in band gap may also reflect increased structural disorder within the polymer network induced by nanoparticle dispersion [26,27].

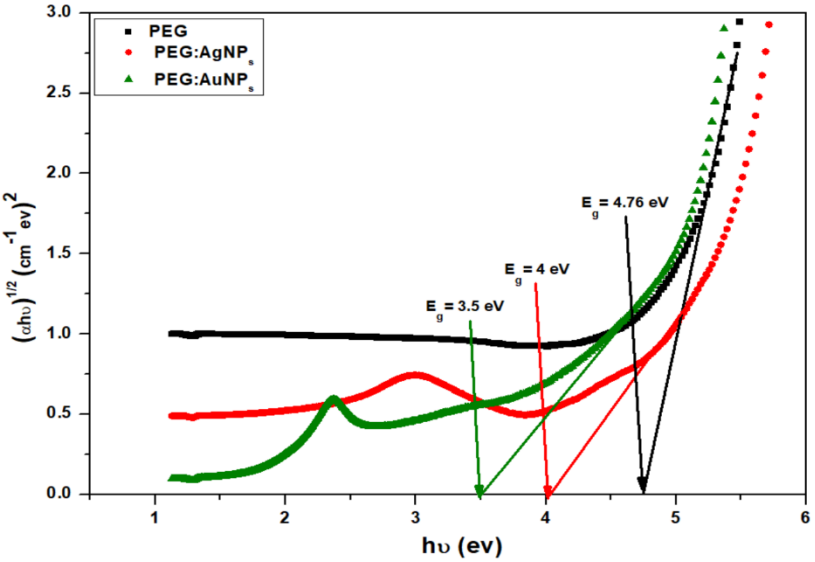

Fig. 3. $(\alpha h\upsilon)^{1/2}$ versus photon energy to illustrate Tauc method

3.3 FESEM

Figures 4(a),4 (b) illustrate solution samples in which silver and gold nanoparticles are uniformly dispersed within a PEG-based polymer matrix. The PEG polymer is initially colorless, then gradually changes color to light yellow with the formation of silver nanoparticles and to light pink with the formation of gold nanoparticles. As the concentration and particle size increase over time, the solution becomes dark yellow in the presence of silver nanoparticles and dark red in the presence of gold nanoparticles, where the solutions were deposited on a glass slide of dimensions (1cm×1cm). Figures 4(a), and 4(b) show microscopic images illustrating the morphology and size distribution of the nanoparticles within the PEG-based polymer matrix. The particle size distribution was analyzed using ImageJ software. Furthermore, the surface of the biomaterial treated with silver and gold nanoparticles exhibits fewer pores compared to the untreated sample, indicating nanoparticle accumulation within the protrusion-like cavities of the surface structure. The FESEM micrographs illustrated in Figures 4(a) and 4(b) indicate the morphological modification induced by the silver and gold nanoparticle treatment. The surface morphology, particle distribution, and visual homogeneity suggest the effective role of the PEG matrix in stabilizing the nanoparticles. The surface exhibits a well-defined, network-like architecture with a highly homogeneous distribution of nanoparticles within the polymer matrix. The uniform dispersion of the particles, characterized by the absence of significant agglomeration, confirms the effective role of the PEG matrix in stabilizing the nanoparticles, the observed average particle size distribution demonstrates structural uniformity, as the nanoparticles are successfully accommodated within the surface cavities, leading to a notable reduction in surface porosity compared to the untreated control. produced surface appears more uniform, demonstrating the nearly total influence of the two chemical processes. Additionally, PEG was used to immobilize or

install the nanoparticles of silver and gold, which prevented them from aggregating. This resulted in a highly homogeneous layer of silver nanoparticles and gold nanoparticles on the surface of the polymer film [28,29].

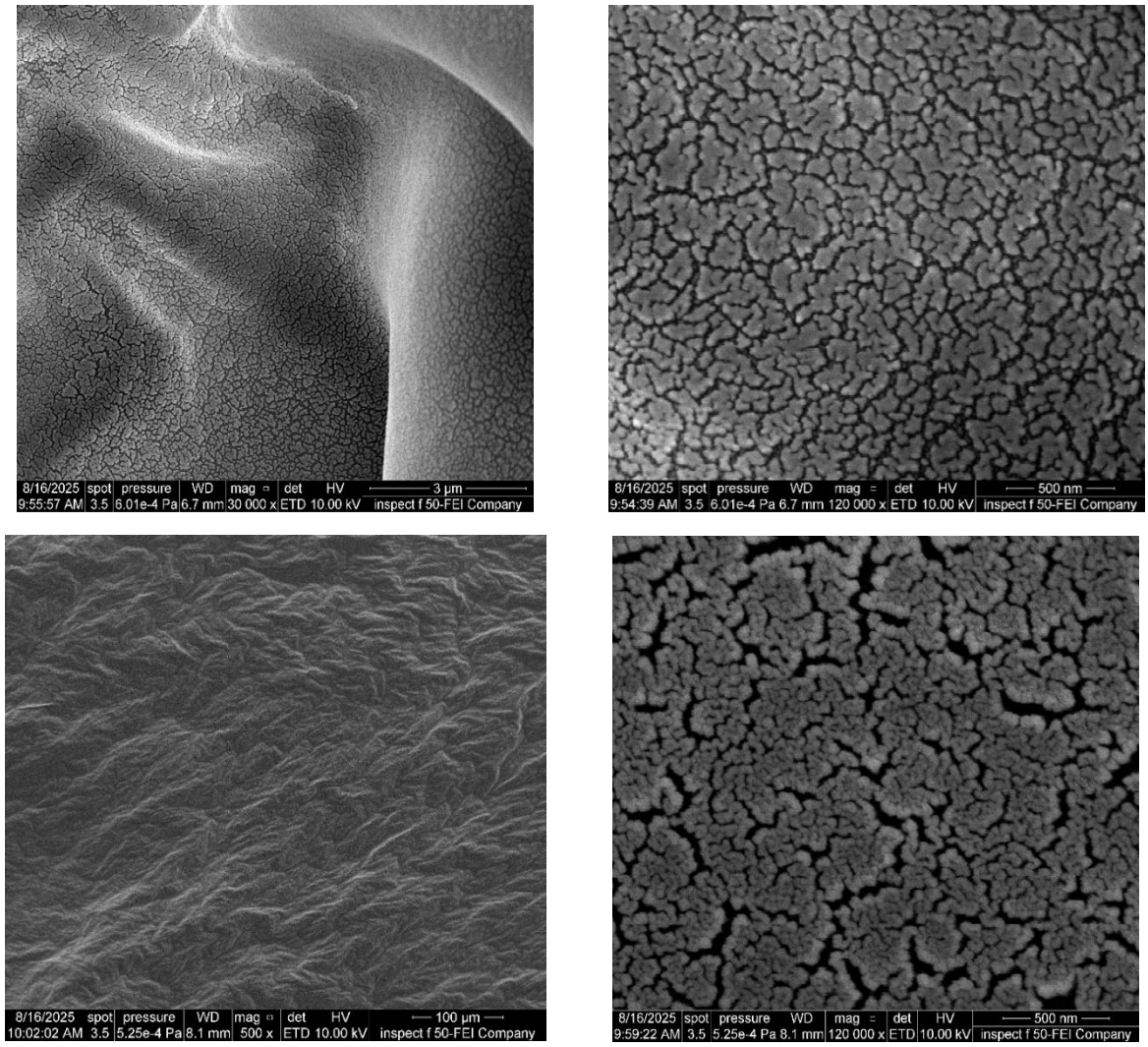

(a)

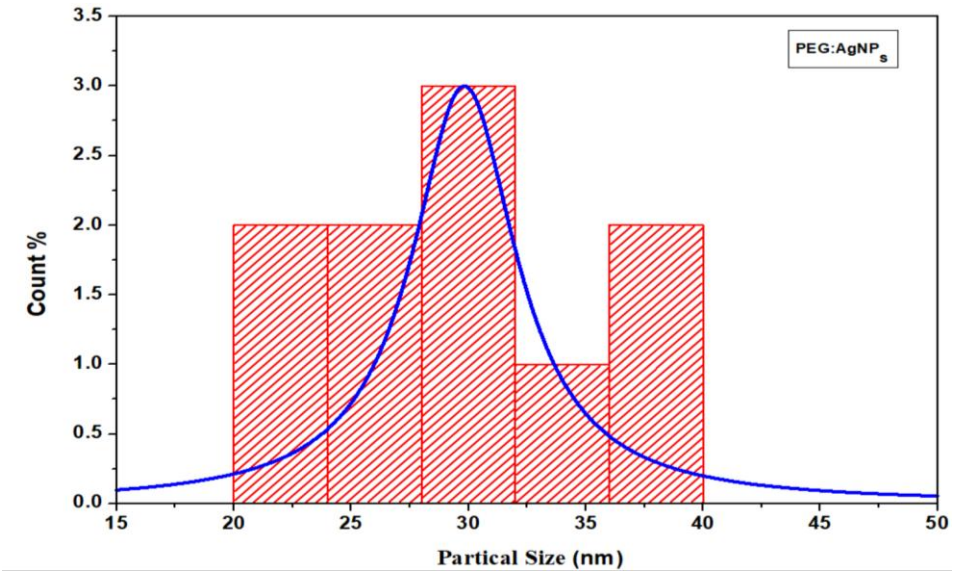

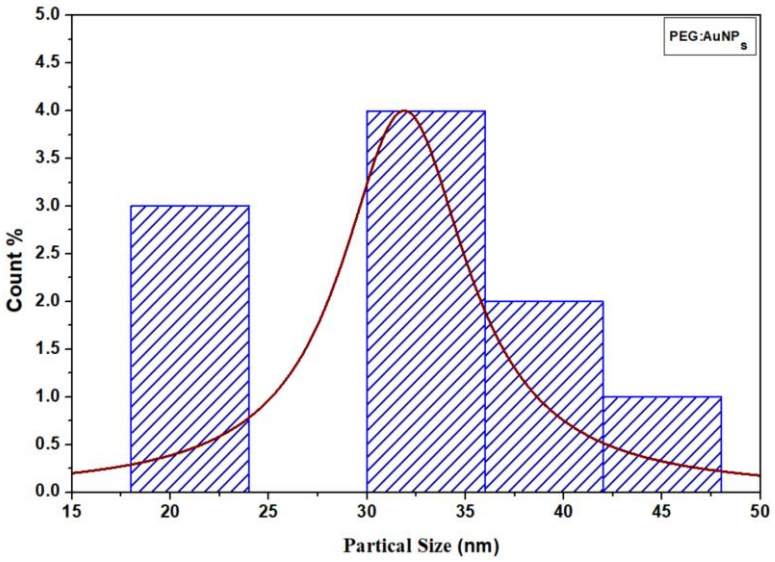

(b)

Fig. 4. (a) FESEM images and statistical distribution of PEG: AgNPs and (b)FESEM images and statistical distribution of PEG: AuNPs

3.4 Antimicrobial Activity Tests

Fig.5 illustrates the antibacterial activity of the fabricated PEG-based composite films against (S. aureus, E. faecalis, E. coli and K. pneumoniae). The inhibition zones given in Table (1) are average antimicrobial inhibition diameters under the prepared PEG/AgNPs and PEG/AuNPs films. Fig. (5), the photographs of the tested biomaterials after 48 h incubation time were shown in Fig.5. Across all panels, inhibition zones decreased progressively with concentration, indicating clear concentration-dependent activity. At 100, material PEG/AuNPs exhibited the largest zones against S. aureus (32 mm) and S. faecalis (30 mm), exceeding those of PEG: AgNPs (28 mm and 25 mm, respectively). Based on the observed inhibition zone diameters, the tested PEG-based composite films showed varying degrees of antimicrobial activity. Throughout the concentration range, the inhibition zones for PEG/AuNPs films were consistently larger than those observed for PEG/AgNPs films across the studied bacterial strains. Statistical analysis using two-way ANOVA confirmed that these differences are statistically significant ($\rho < 0.05$), supporting the enhanced antimicrobial efficacy of the PEG/AuNPs) formulation. These results suggest a concentration-dependent trend in the antimicrobial effectiveness of the prepared films, the statistical significance of which was confirmed by two-way ANOVA analysis. for instance, regarding E. coli, zones fell from 24 mm (PEG/AuNPs /100) to 20 mm (PEG/AuNPs /12.5) versus 23 → 15 mm for PEG: AgNPs; for K. pneumoniae, 26 → 19 mm (PEG/AuNPs) versus 25 → 21 mm (PEG: AgNPs). By organism, S. aureus was the most susceptible to both PEG: AgNPs and PEG/AuNPs across the concentration range, with PEG: AuNPs maintaining a ~2–4 mm advantage at each dilution and retaining a relatively large zone (20–23 mm) even at 12.5 μg/mL. S. faecalis showed lower zones overall than S. aureus but still displayed strong susceptibility to PEG: AuNPs (30 → 19 mm) compared with PEG: AgNPs (25 → 15 mm). Among Gram-negatives, K. pneumoniae appeared more susceptible than E. coli across agents and concentrations, E. coli exhibited the smallest zones within the PEG: AgNPs and PEG: AuNPs panels (e.g., PEG: AgNPs 23 → 15 mm, PEG: AuNPs 24 → 20 mm), consistent with relatively higher intrinsic resistance.

The antibacterial activity of PEG/Ag and PEG/Au formulations based on the mean inhibition zone diameter. All experiments were performed in three independent replicates and data are expressed as mean ± standard deviation (SD) in millimeters. As shown in table 1, the standard deviation for all samples was consistently less than 1.0 mm, indicating high experimental reproducibility. Statistical analysis confirmed that the differences across the tested concentrations are significant ($\rho < 0.05$).

Table 1. Antibacterial activity of PEG/Ag and PEG/Au formulations based on the mean inhibition zone diameter

Concentrations	S. aureus	E. faecalis	E. coli	K. pneumoniae
PEG/Ag / 100	28.00 ± 0.35	24.88 ± 0.29	23.28 ± 0.15	24.91 ± 0.48
PEG/Ag / 75	25.00 ± 0.17	23.29 ± 0.45	21.26 ± 0.31	24.12 ± 0.22
PEG/Ag / 50	23.09 ± 0.25	18.89 ± 0.37	18.97 ± 0.22	22.75 ± 0.39
PEG/Ag / 25	20.09 ± 0.35	16.83 ± 0.17	17.10 ± 0.34	21.97 ± 0.26
PEG/Ag / 12.5	17.83 ± 0.23	14.73 ± 0.24	15.29 ± 0.40	20.87 ± 0.31
PEG/Au / 100	31.89 ± 0.25	29.98 ± 0.30	23.81 ± 0.32	26.45 ± 0.46
PEG/Au / 75	28.19 ± 0.23	26.54 ± 0.26	22.56 ± 0.19	23.86 ± 0.50
PEG/Au / 50	25.51 ± 0.40	23.79 ± 0.27	22.17 ± 0.38	22.20 ± 0.26
PEG/Au / 25	23.01 ± 0.32	20.12 ± 0.19	21.18 ± 0.34	19.83 ± 0.36
PEG/Au / 12.5	19.98 ± 0.14	19.11 ± 0.20	19.78 ± 0.29	19.28 ± 0.39

Note: Values are presented as mean ± standard deviation of three replicates and are expressed in millimeters (mm).

Table 2. Two-way analysis of variance of the effects of nanoparticle type and concentration on inhibition zone diameter

Bacterial species	Source of variation	F (df)	p-value	Partial η^2
Staphylococcus aureus	Nanoparticle type (Ag vs. Au)	805.07 (1, 20)	<0.001	0.976
	Concentration	1400.06 (4, 20)	<0.001	0.996
	Nanoparticle type × concentration	8.78 (4, 20)	<0.001	0.637
Enterococcus faecalis	Nanoparticle type (Ag vs. Au)	1599.33 (1, 20)	<0.001	0.988
	Concentration	1397.56 (4, 20)	<0.001	0.996
	Nanoparticle type × concentration	14.02 (4, 20)	<0.001	0.737
Escherichia coli	Nanoparticle type (Ag vs. Au)	604.12 (1, 20)	<0.001	0.968
	Concentration	357.17 (4, 20)	<0.001	0.986
	Nanoparticle type × concentration	48.92 (4, 20)	<0.001	0.907
Klebsiella pneumoniae	Nanoparticle type (Ag vs. Au)	19.14 (1, 20)	<0.001	0.489
	Concentration	221.44 (4, 20)	<0.001	0.978
	Nanoparticle type × concentration	21.50 (4, 20)	<0.001	0.811

The two-way ANOVA demonstrated that the antibacterial activity of PEG/Ag and PEG/Au formulations was significantly influenced by nanoparticle type, concentration, and, in most cases, the interaction between these two factors. This indicates that the antibacterial response was not determined by the metallic nanoparticle alone, but also depended on the concentration at which each formulation was tested and on the susceptibility profile of the bacterial species.

In case of *Staphylococcus aureus*, both nanoparticle type and concentration exerted highly significant effects on inhibition zone diameter. The significant interaction term further indicates that the difference between PEG/Au and PEG/Ag changed across the tested concentrations. The PEG/Au showed greater antibacterial activity against *S. aureus*, particularly at higher concentrations. This may reflect a more effective interaction of gold-containing nanoparticles with the exposed peptidoglycan-rich cell envelope of this Gram-positive species, although the observed activity may also be influenced by particle size, surface charge, aggregation state, and dispersion within the PEG matrix.

For *Enterococcus faecalis*, the very large effect sizes for nanoparticle type and concentration suggest that both variables strongly contributed to differences in antibacterial activity. PEG/Au consistently produced larger inhibition zones than PEG/Ag, indicating a stronger activity against *E. faecalis* under the present experimental conditions. However, this interpretation should remain formulation-specific because nanoparticle activity is influenced by physicochemical characteristics, including particle morphology, surface functionalization, and the ability of the polymeric carrier to maintain nanoparticle dispersion.

Escherichia coli, the significant interaction between nanoparticle type and concentration was particularly notable. This result indicates that the relative activity of PEG/Au and PEG/Ag was not constant across all concentrations. PEG/Au appeared to retain comparatively stronger activity at lower and intermediate concentrations, whereas the difference between the two formulations was smaller at the highest concentration. Such variability may be related to the outer membrane barrier of Gram-negative bacteria, which can alter nanoparticle penetration and influence the diffusion of active components through the agar medium.

In *Klebsiella pneumoniae*, concentration remained a highly significant determinant of antibacterial activity. However, the interaction between nanoparticle type and concentration showed that the superiority of one formulation over the other was concentration-dependent. PEG/Au showed greater activity at the highest concentration, whereas PEG/Ag tended to maintain comparatively better activity at some lower concentrations. This complex response may be associated with the structural characteristics of *K. pneumoniae*, including its outer membrane, capsular material, and reduced permeability, all of which may influence the interaction between bacterial cells and metallic nanoparticles.

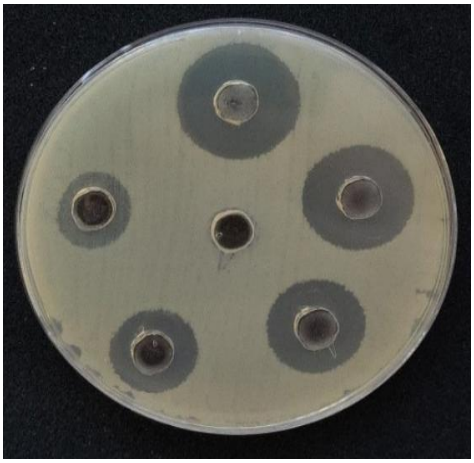

S. aureus

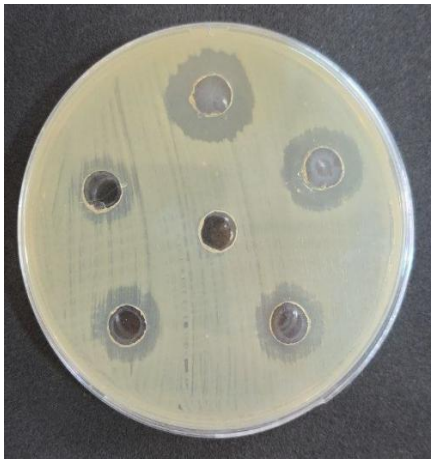

E. faecalis

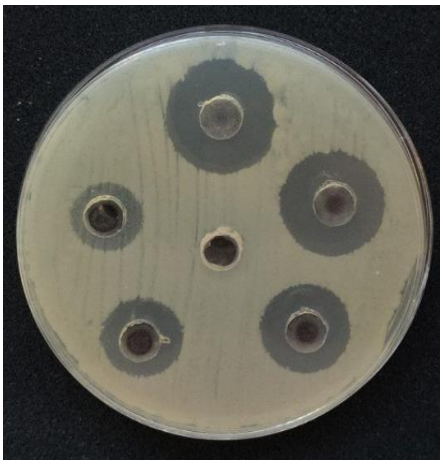

E. coli

K. pneumoniae

(a)

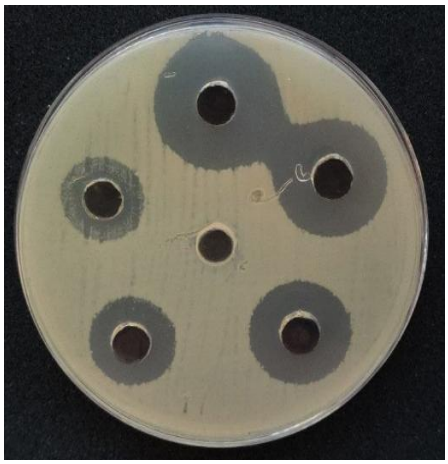

S. aureus

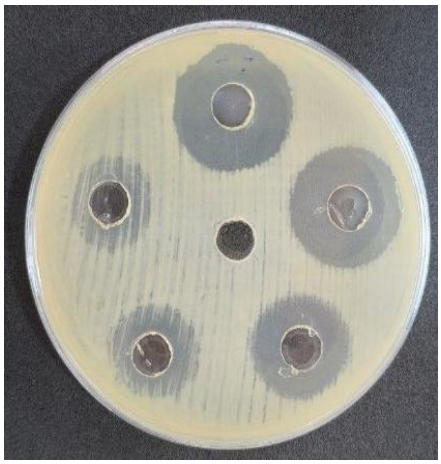

E. faecalis

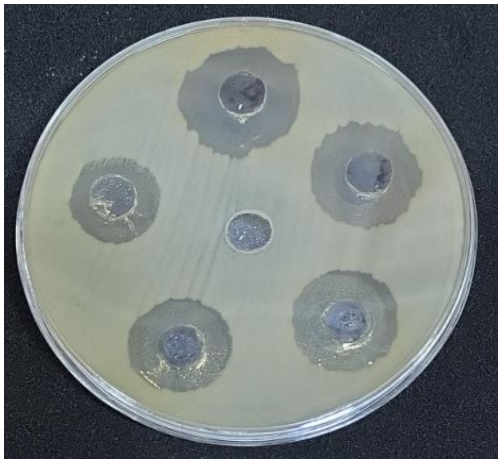

E. coli

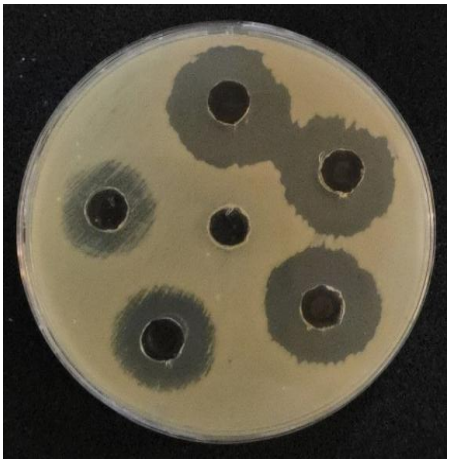

K. pneumoniae

(b)

Fig. 5. (a) Antibacterial activity images of PEG: Ag NPs composite against (*S. aureus , E. faecalis , E.coli and K. pneumoniae)and* (b): Antibacterial activity images of PEG:Au NPs composite against (*S. aureus , E. faecalis, E.coli and K. pneumoniae)*

4. Conclusion

In this study, PEG/AgNPs and PEG/AuNPs nanocomposites were successfully synthesized. FESEM and spectroscopic analyses confirmed the uniform incorporation of nanoparticles within the PEG matrix. The antibacterial evaluation demonstrated that the inhibition zone diameters for the synthesized films ranged from 15 mm to 32 mm across the tested bacterial strains (S. aureus, E. faecalis, E. coli, and K. pneumoniae), with activity showing a clear positive correlation with nanoparticle concentration. While these results indicate promising antibacterial potential, the study is limited by its in vitro nature. Future research, specifically regarding cytotoxicity and long-term release kinetics, is necessary to transition these findings toward clinical application.

References

[1] Suhail M, Ramadan AA, Aziz SB, Abdullah OG. Chemical surface treatment with toluene to enhances sensitivity of NO2 gas sensor based on CuPc Ts/Alq3 thin films. J Sci Adv Mater Devices. 2017; 2(3): 301-308. https://doi.org/10.1016/j.jsamd.2017.07.003

[2] Abdulameer AF, Suhail M, Abdullah OG, Al-Essa IM. Fabrication and characterization of NiPcTs organic semiconductors based surface type capacitive-resistive humidity sensors. J Mater Sci Mater Electron. 2017; 28(18): 13472-13477. https://doi.org/10.1007/s10854-017-7186-x
[3] Brogly M, Bistac S, Bindel D. Adsorption and structuration of PEG thin films: Influence of the substrate chemistry. Polymers. 2024; 16(9): 1244. https://doi.org/10.3390/polym16091244
[4] Abdullah SS, Ahmed FL, Jasim SK. Structural and optical studies on silver nitrate doped polymer blend and effect on some pathogenic bacteria. Rev Mex Fis. 2025; 71(4): 041004. https://doi.org/10.31349/RevMexFis.71.041004
[5] Salman SA, Bakr NA, Abduallah SS. Study of thermal decomposition and FTIR for PVA-AlCl composite films. J Eng Appl Sci. 2019; 14(3): 717-724. https://doi.org/10.36478/jeasci.2019.717.724
[6] Abdulkadhim SM, Hashim FS, Rabee BH. Synthesis of (PVA-PVP: ZnO and Ag) nanocomposite films: Characterization and antibacterial application. NeuroQuantology. 2022; 20(1): 738-745.
[7] Hassanen EI, Morsy EA, Hussien AM, Ibrahim MA, Farroh KY. The effect of different concentrations of gold nanoparticles on growth performance, toxicopathological and immunological parameters of broiler chickens. Biosci Rep. 2020; 40(3): BSR20194296. https://doi.org/10.1042/BSR20194296
[8] Sengani M, Grumezescu AM, Rajeswari VD. Recent trends and methodologies in gold nanoparticle synthesis-A prospective review on drug delivery aspect. OpenNano. 2017; 2: 37-46. https://doi.org/10.1016/j.onano.2017.07.001
[9] Cepoi L, Zinicovscaia I, Rudi L, Chiriac T, Rotari I, Turchenko V, et al. Effects of PEG-coated silver and gold nanoparticles on Spirulina platensis biomass during its growth in a closed system. Coatings. 2020; 10(8): 717. https://doi.org/10.3390/coatings10080717
[10] Elahi N, Kamali M, Baghersad MH. Recent biomedical applications of gold nanoparticles: A review. Talanta. 2018; 184: 537-556. https://doi.org/10.1016/j.talanta.2018.02.088
[11] Cabuzu D, Cirja A, Puiu R, Grumezescu AM. Biomedical applications of gold nanoparticles. Curr Top Med Chem. 2015; 15(16): 1605-1613. https://doi.org/10.2174/1568026615666150414144750
[12] Guo J, Rahme K, He Y, Li LL, Holmes J, O'Driscoll C. Gold nanoparticles enlighten the future of cancer theranostics. Int J Nanomedicine. 2017; 12: 6131-6152. https://doi.org/10.2147/IJN.S140772
[13] Sharma N, Pinnaka AK, Raje M, Fnu A, Bhattacharyya MS, Choudhury AR. Exploitation of marine bacteria for production of gold nanoparticles. Microb Cell Fact. 2012; 11: 86. https://doi.org/10.1186/1475-2859-11-86
[14] Calderón-Jiménez B, Johnson ME, Montoro Bustos AR, Murphy KE, Winchester MR, Vega Baudrit JR. Silver nanoparticles: Technological advances, societal impacts, and metrological challenges. Front Chem. 2017; 5: 6. https://doi.org/10.3389/fchem.2017.00006
[15] Rai M, Yadav A, Gade A. Silver nanoparticles as a new generation of antimicrobials. Appl Microbiol Biotechnol. 2009; 84(2): 277-287. https://doi.org/10.1016/j.biotechadv.2008.09.002
[16] Morones JR, Elechiguerra JL, Camacho A, Holt K, Kouri JB, Ramírez JT, et al. The bactericidal effect of silver nanoparticles. Nanotechnology. 2005; 16(10): 2346-2353. https://doi.org/10.1088/0957-4484/16/10/059
[17] Marambio-Jones C, Hoek EMV. A review of the antibacterial effects of silver nanomaterials and potential implications for human health and the environment. J Nanopart Res. 2010; 12(5): 1531-1551. https://doi.org/10.1007/s11051-010-9900-y
[18] Nitiică Ş, Moldovan AI, Toma V, Moldovan CS, Berindan-Neagoe I, Ştiufiuc G, et al. PEGylated gold nanoparticles with interesting plasmonic properties synthesized using an original, rapid, and easy-to-implement procedure. J Nanomater. 2018; 2018: 1-7. https://doi.org/10.1155/2018/5954028
[19] Shameli K, Bin Ahmad M, Jazayeri SD, Sedaghat S, Shabanzadeh P, Jahangirian H, et al. Synthesis and characterization of polyethylene glycol mediated silver nanoparticles by the green method. Int J Mol Sci. 2012; 13(6): 6639-6650. https://doi.org/10.3390/ijms13066639
[20] Todica M, Stan O, Pop CV, Răzvan Ş, Niculaescu C. Investigation of polyethylene glycol with embedded gold nanoparticles membranes. Rom J Phys. 2020; 65(7-8): 702.
[21] Sarkar K, Banerjee SL, Kundu PP, Madras G, Chatterjee K. Biofunctionalized surface-modified silver nanoparticles for gene delivery. J Mater Chem B. 2015; 3(26): 5266-5276. https://doi.org/10.1039/C5TB00614G
[22] Toderas F, Baia M, Baia L, Astilean S. Photothermal properties of gold nanoparticles for biomedical applications. Nanotechnology. 2007; 18(25): 255702. https://doi.org/10.1088/0957-4484/18/25/255702
[23] Morales-Avila E, Ferro-Flores G, Ocampo-García BE, López-Téllez G, López-Ortega J, Rogel-Ayala DG, et al. Multimodal 99mTc-labeled gold nanoparticles for biomedical applications. J Nanomater. 2017; 2017: 8501268. https://doi.org/10.1155/2017/5831959
[24] Alkilany AM, Yaseen AB, Kailani MH. Synthesis and characterization of gold nanoparticles functionalized with polyethylene glycol and cysteine. J Nanomater. 2015; 2015: 582496. https://doi.org/10.1155/2015/712359

[25] Ghanipour M, Dorranian D. Effect of Ag-nanoparticles doped in polyvinyl alcohol on the structural and optical properties of PVA films. J Nanomater. 2013; 2013: 689530. https://doi.org/10.1155/2013/897043
[26] Devi CU, Sharma AK, Rao VVRN. Electrical and optical properties of pure and silver nitrate-doped polyvinyl alcohol films. Mater Lett. 2002; 56(3): 167-174. https://doi.org/10.1016/S0167-577X(02)00434-2
[27] Rozra J, Saini I, Sharma A, Chandak N, Aggarwal S, Sharma PK. Cu nanoparticles induced structural, optical and electrical modification in PVA. Mater Chem Phys. 2012; 134(2-3): 1121-1126. https://doi.org/10.1016/j.matchemphys.2012.04.004
[28] Abdelaziz M. Cerium (III) doping effects on optical and thermal properties of PVA films. Physica B. 2011; 406(6-7): 1300-1307. https://doi.org/10.1016/j.physb.2011.01.021
[29] Ragaseema VM, Unnikrishnan S, Kalliyana Krishnan V, Krishnan LK. The antithrombotic and antimicrobial properties of PEG-protected silver nanoparticle coated surfaces. Biomaterials. 2012; 33(11): 3083-3092. https://doi.org/10.1016/j.biomaterials.2012.01.005
[30] Karademir F, Ayhan F. Antimicrobial surface functionality of PEG coated and AgNPs immobilized extracorporeal biomaterials. Biointerface Res Appl Chem. 2022; 12(1): 1039-1052. https://doi.org/10.33263/BRIAC121.10391052